Two-step photocatalytic water splitting into H(2) and O(2) using layered metal oxide KCa(2)Nb(3)O(10) and its derivatives as O(2)-evolving photocatalysts with IO(3)[−]/I[−] or Fe[3+]/Fe[2+] redox mediator

AUTHOR(S):

Suzuki, Hajime; Tomita, Osamu; Higashi, Masanobu; Abe, Ryu

Journal Name

RSCPublishing

ARTICLE

Cite this: DOI: 10.1039/xoxxoooooox

Received ooth January 2012,
Accepted ooth January 2012

DOI: 10.1039/xoxxoooooox

www.rsc.org/

Two-step photocatalytic water splitting into H_2 and O_2 using layered metal oxide $KCa_2Nb_3O_{10}$ and its derivatives as O_2-evolving photocatalysts with IO_3^-/I^- or Fe^{3+}/Fe^{2+} redox mediator

Hajime Suzuki,[a] Osamu Tomita,[a] Masanobu Higashi,[a] Ryu Abe*[a,b]

Two-step photoexcitation (Z-scheme) systems that can split water into H_2 and O_2 under UV light were constructed using a layered potassium calcium niobate ($KCa_2Nb_3O_{10}$) and its derivatives as O_2-evolving photocatalysts, combined with an appropriate H_2-evolving photocatalyst in the presence of iodate/iodide (IO_3^-/I^-) or iron(III)/(II) (Fe^{3+}/Fe^{2+}) as an electron mediator. The original $KCa_2Nb_3O_{10}$ showed negligibly low activity for photocatalytic water oxidation to O_2 in the presence of IO_3^- as an electron acceptor, since the anionic IO_3^- cannot penetrate into the interlayer spaces owing to the strong electrostatic repulsion between IO_3^- and the negatively charged niobate layers. The rate of O_2 evolution was significantly increased after exfoliation-restack process of $KCa_2Nb_3O_{10}$, certainly due to much-facilitated access of IO_3^- to the opened reduction sites of nanosheet surfaces. The loading of RuO_x or PtO_x cocatalysts on the samples significantly increased the rate of O_2 evolution. The electrochemical analysis indicated that these cocatalysts effectively decreased the overpotential of IO_3^- reduction, which occurs through the 6-electron process. On the other hand, the original layered structure was effective for the photocatalytic O_2 evolution in the presence of Fe^{3+} electron acceptor even without any cocatalysts, suggesting that the interlayer spaces of layered niobate can work as effective reduction sites for cationic Fe^{3+}. Finally, simultaneous evolution of H_2 and O_2 was attempted by using these $KCa_2Nb_3O_{10}$-based materials as O_2-evolving photocatalysts, combined with an appropriate H_2-evolving photocatalyst. By employing the appropriate combination of $KCa_2Nb_3O_{10}$-based materials with the redox couple, which was suggested by the result of half O_2-evolution reactions, simultaneous evolution of H_2 and O_2 stably proceeded with higher rates.

1. Introduction

Photocatalytic water splitting using semiconductor materials have received much attention due to the potential for clean production of H_2 from water by harvesting abundant solar light. To achieve practically high efficiency of H_2 production under solar light irradiation, both the utilization of wide range of solar light spectrum, especially in visible light region, and the high quantum efficiency in the reaction are undoubtedly indispensable. Water splitting systems based on two-steps photoexcitation, which were inspired by the Z-scheme mechanism of photosynthesis in green plants, have been recently developed and proven as an effective way to utilize wider range of visible light.[1-13] In this system, the water-splitting reaction is broken up into two stages, one for H_2 evolution and the other for O_2 evolution, and these are combined by using a shuttle redox couple in the solution. The present author's group have first demonstrated visible-light-induced water splitting into H_2 and O_2 using two different metal oxide semiconductors and an iodate/iodide (IO_3^-/I^-)[1], and have applied various kinds of semiconductor materials, not only metal oxides but also metal oxynitrides[2-6] and organic dyes,[7, 8] to the two-steps (Z-scheme) water splitting system. Kudo and his coworkers have also demonstrated Z-scheme type water splitting under visible light using metal oxide photocatalysts with redox couples such as Fe^{3+}/Fe^{2+} [9-11] and $Co(bpy)_3^{3+}/Co(bpy)_3^{2+}$, [12] or even without any redox couple in the solution (through direct electron transfer between semiconductor particles)[13].

Cation-exchangeable layered metal oxides such as $K_4Nb_6O_{17}$ have been studied as promising candidates for efficient photocatalyst materials for water splitting.[14-33] They

generally consist of 2-dimentional anion layers of metal oxide and the cations such as K^+ that compensate the negative charge of anion layers, thus forming cation-exchangeable layered structures. Efficient photocatalytic reactions are expected to proceed on such cation-exchangeable layered metal oxides, because water molecules, as well as small cations, can generally intercalate into the interlayer spaces of them and efficiently react with the photoexcited carriers, which are generated on the semiconducting 2-dimentional anion layers of metal oxides. Indeed, some cation-exchangeable layered metal oxides such as $K_4Nb_6O_{17}$,[23-25] $K_2La_2Ti_3O_{10}$,[26, 27] $Rb_4Ta_6O_{17}$,[28] $RbNdTa_2O_7$,[29, 30] $A'_2ASrTa_2O_7$ (A'= H or K, A= $La_{2/3}$ or Sr),[31, 32] $NaCa_2Ta_3O_{10}$[33] have been reported as active photocatalyst for efficient water splitting into H_2 and O_2 under UV irradiation. Among them, layered perovskite structure can offer us great variety of semiconducting materials, including visible-light-responsive ones, based on the facile exchange of cations in the A and B sites within the appropriate parameters of tolerance factor.[34-36] Partial replacement of cations and/or exfoliation of the 2-dimentional layers of these layered perovskite materials have also been extensively studied to enhance the photocatalytic activity. However, such cation-exchangeable layered metal oxides have not been employed as photocatalysts in the Z-scheme water-splitting systems, to the best of our knowledge.

One of the Dion-Jacobson type layered perovskite, $KCa_2Nb_3O_{10}$ has been reported to show significantly high activity for photocatalytic H_2 evolution from an aqueous methanol solution under UV light after exchange of the K^+ cations in the interlayer by protons (H^+), whereas it showed negligibly low activity for O_2 evolution in the presence of Ag^+ ion as sacrificial electron acceptor.[37] Ebina *et al*. have reported simultaneous evolution of H_2 and O_2 on derivatives of $KCa_2Nb_3O_{10}$ that were prepared *via* exfoliation of 2-dimentional layers with a soft-chemical method and following restack process, in which nanoparticles of RuO_x cocatalysts were simultaneously incorporated between the 2-dimentional niobate layers.[38] This finding implies that the niobate layers of $KCa_2Nb_3O_{10}$ are potentially capable of oxidation of water efficiently. In the present study, we thus focused on the utilization of $KCa_2Nb_3O_{10}$ and its derivatives as O_2-evolving photocatalysts in the Z-scheme water-splitting systems with redox mediator such as IO_3^-/I^- or Fe^{3+}/Fe^{2+}. The influences of exfoliation-restack and cocatalysts loading on the activity and selectivity of water oxidation were examined in detail.

2. Experimental

2-1. Preparation of photocatalysts.

Particles of $KCa_2Nb_3O_{10}$ were prepared by calcining a mixture of K_2CO_3, $CaCO_3$ and Nb_2O_5 (K:Ca:Nb = 1.1:2:3) at 1473 K for 12 h. The obtained $KCa_2Nb_3O_{10}$ powder was stirred with 5 M HNO_3 aqueous solution for 72 h to replace K^+ to H^+, washed with distilled water, and then dried in air at room temperature. The proton-exchanged particles will be denoted as $H^+/KCa_2Nb_3O_{10}$ hereafter. The $H^+/KCa_2Nb_3O_{10}$ particles (0.4 g) were suspended in 100 mL of aqueous solution, in which equimolar of tetrabutylammonium hydroxide (TBAOH) molecules to that of $H^+/KCa_2Nb_3O_{10}$ (ca. 0.73 mmol, calculated as $HCa_2Nb_3O_{10}\cdot 1.5H_2O$) was added as an initiator of exfoliation. The suspension was continuously shaken at room temperature for 7 days until the $H^+/KCa_2Nb_3O_{10}$ exfoliate into nanosheets.[38] The resulting colloidal suspension was added dropwise into 2 M KOH aqueous solution, immediately producing white precipitate. The precipitate was thoroughly washed with water several times and dried in air at room temperature; the obtained sample will be denoted as ex-$Ca_2Nb_3O_{10}/K^+$ hereafter. The TEM images of the exfoliated nano sheets and the ex-$Ca_2Nb_3O_{10}/K^+$ are shown in Fig. S1 in supporting information (SI). Modification of ex-$Ca_2Nb_3O_{10}/K^+$ with cocatalysts was carried out by impregnation of an aqueous solution containing one of ammine complexes of metals such as $[Pt(NH_3)_4](OH)_2$, $[(NH_3)Ru\text{-}O\text{-}Ru(NH_3)_4\text{-}O\text{-}Ru(NH_3)_5]Cl_6$, $[Ir(NH_3)_6]Cl_3$, $[Rh(NH_3)_6]Cl_3$ and $[Co(NH_3)_6]Cl_3$, followed by heating in air at 773 K for 1 h. Since the dominant valence states of these metal species after the loading procedure were confirmed to be Pt^{2+}, Ru^{4+}, Ir^{4+}, and Rh^{3+} by X-ray photoabsorption spectroscopy (XPS, ULVAC Phai MT-5500), the samples loaded with the cocatalysts will be denoted as PtO, RuO_2, IrO_2 and Rh_2O_3-loaded one, respectively. On the other hand, the samples loaded with Co species were confirmed to contain both Co^{2+} and Co^{3+} states, therefore will be denoted as CoO_x-loaded one for simplification. The products will be denoted as $MO_y/ex\text{-}Ca_2Nb_3O_{10}/K^+$ (MO_y = PtO, RuO_2, IrO_2, Rh_2O_3 and CoO_x). When the protonated forms of these samples are required, the K^+ cations exist in $MO_y/ex\text{-}Ca_2Nb_3O_{10}/K^+$ samples were replaced with H^+ by stirring in an aqueous HNO_3 solution (1 M) at room temperature for 24 h (referred to as $MO_y/ex\text{-}Ca_2Nb_3O_{10}/K^+/H^+$).

Strontium titanate doped with rhodium species ($SrTiO_3$:Rh)[36] was prepared by solid state reaction. A mixture of $SrCO_3$, TiO_2 and Rh_2O_3 (Sr : Ti : Rh = 1 : 0.99 : 0.01 to form ideal formula of $SrTi_{0.99}Rh_{0.01}O_{3-\delta}$) was calcined in air at 873 K for 2 h and subsequently at 1273 K for 10 h. Pt cocatalyst was loaded onto $SrTiO_3$:Rh by impregnation using $H_2PtCl_6\cdot 6H_2O$ and subsequent heating under a H_2 flow at 573 K for 2 h. In the case of Ru cocatalyst, Ru species were loaded on $SrTiO_3$:Rh by means of photodeposition method using $RuCl_3\cdot nH_2O$ as a Ru source, according to the method reported previously.[11]

2-2. Photocatalytic reactions.

Photocatalytic reactions were carried out using a Pyrex glass reactor connected to a closed gas–circulation system. For the photocatalytic water oxidation (O_2 evolution) in the presence of an electron accepter (i.e., half reaction of water splitting) catalyst powder (50 or 100 mg) was suspended in 70 mL of an aqueous $NaIO_3$ or $Fe(NO_3)_3$ solution (5 mM) in the reactor by using a set of magnetic stirrer and bar. The pH values of the solutions were controlled by adding aqueous KOH or HNO_3 solution, when needed. Since it was demonstrated that the O_2

evolution in the presence of IO_3^- generally proceeded more efficiently in basic conditions (above pH 9), the original $KCa_2Nb_3O_{10}$ and its derivatives (100 mg) were suspended to $NaIO_3$aq. without proton-exchange. The addition of these K^+-contain samples spontaneously change the pH of $NaIO_3$aq. (originally ca. 6.8) to higher values up to ca. 9.6 due to the exchange of K^+ with H^+ in the solutions. As for the O_2 evolution in the presence of Fe^{3+} electron acceptor, the reaction must be carried out in acidic condition with pH below ca. 3, because Fe^{3+} cations easily precipitate as $Fe(OH)_3$ with higher pH values. In order to maintain the pH values below 3 stably through the reactions, the $KCa_2Nb_3O_{10}$–derivatives were treated by HNO_3aq. before the use as described above, and furthermore a small amount of HNO_3aq. was added into $Fe(NO_3)_3$aq. to adjust the pH to 2.5 before reaction.

For the two-step water-splitting reaction with IO_3^-/I^- redox couple, the Pt-loaded $SrTiO_3$:Rh (50 mg) and one of the $KCa_2Nb_3O_{10}$–derivatives (100 mg) were suspended in an aqueous KI solution (5 mM, 70 mL) as H_2-evolving and O_2-evolving photocatalysts, respectively. The pH value of the solution was adjusted to be ca. 12 by adding small amount of aqueous KOH solution. In the case of two-step water splitting with Fe^{3+}/Fe^{2+} redox couple, the Ru-loaded $SrTiO_3$:Rh (50 mg) and one of the proton-exchanged $KCa_2Nb_3O_{10}$–derivative (500 mg) were suspended in 250 mL of an aqueous $Fe(ClO_4)_2$ solution (5 mM), whose pH values were adjusted to ca. 2.5 by adding a small amount of aqueous $HClO_4$ solution. The suspension was irradiated using 300 W Xe lamp (Cermax LF-300F, $\lambda > 300$ nm) thorough a water filter. The evolved gases were analyzed by on-line gas chromatography (detector; TCD, column packing; molecular sieve 5 A, Ar carrier).

2-3. Electrochemical Measurement.

To evaluate the catalytic ability of metal oxides (PtO, RuO_2, IrO_2, Rh_2O_3, and CoO_x) used as cocatalysts, these particles were prepared on conductive glass substrate (FTO) *via* basically same procedure to that on $KCa_2Nb_3O_{10}$–derivatives as follows. Small amount (50 μL) of $[Pt(NH_3)_4](OH)_2$, $[(NH_3)Ru\text{-}O\text{-}Ru(NH_3)_4\text{-}O\text{-}Ru(NH_3)_5]Cl_6$, $[Ir(NH_3)_6]Cl_3$, $[Rh(NH_3)_6]Cl_3$ or $[Co(NH_3)_6]Cl_3$ aqueous solution (10 mM) was dropped on a FTO substrate, and the substrates were dried in air at room temperature and subsequently calcined at 773 K for 1 h. XPS analysis confirmed that the valence states of the loaded metal cations were basically same as to those loaded on the $KCa_2Nb_3O_{10}$–derivatives. The electrochemical cell used for the experiments consisted of a prepared MO_y/FTO electrode as the working electrode, a Pt wire as the counter electrode, and a Ag/AgCl as the reference electrode. The potential of the working electrode was controlled using a potentiostat (VersaSTAT3, Princeton Applied Research Co., Ltd.). The overpotentials for IO_3^- and Fe^{3+} reduction over the MO_y/FTO electrodes were estimated by means of cyclic voltammetry (CV) in a 0.5 M Na_2SO_4 aqueous solution (40 mL) in the absence and presence of $NaIO_3$ or $Fe(NO_3)_3$ with different concentrations. The overpotentials for water oxidation were estimated based on the CV profiles of the MO_y/FTO electrodes in a dehydrated acetonitrile (40 mL) solutions containing tetrabutylammonium perchlorate (0.1 M) and different amounts of distilled water (0, 72, 360, 720 μL).

3. Results and discussion

3-1. Characterizations of samples before and after exfoliation-restack process.

Fig. 1 shows XRD patterns of the prepared samples. Both the original $KCa_2Nb_3O_{10}$ and its proton-exchanged form ($H^+/HCa_2Nb_3O_{10}$) exhibited strong and sharp diffraction peaks corresponding to (00*n*) facets as reported[39, 40], indicating well-regulated stacking of niobate layers along with c-axis. The (00*n*) diffraction peaks shifted to lower angles after the proton-exchange due to the spontaneous hydration of interlayer space, forming average formula of $HCa_2Nb_3O_{10} \cdot 1.5H_2O$.[40] As seen in the SEM images (see Fig. 2-a and b), both the original $KCa_2Nb_3O_{10}$ and $H^+/HCa_2Nb_3O_{10}$ consist of aggregation of plate-like primary particles with grain sizes of several micrometers; these samples exhibit quite small surface area (ca. 0.5 m^2/g) as described in the SEM images. Because the probe N_2 molecule cannot intercalate into quite-narrow space of interlayers, only the outermost part of particles are measured as specific surface area. The intensity of peaks corresponding to (00*n*) was significantly decreased along with obvious broadening in the peak width after the exfoliation-restack process (see Fig. 1-c for ex-$Ca_2Nb_3O_{10}/K^+$ sample). The change in the (00*n*) diffraction peaks indicated that the niobate sheets once exfoliated were randomly restacked by the static attraction between the negatively charged niobate sheet and the positive charge of K^+ cations added into the solution, forming loosely

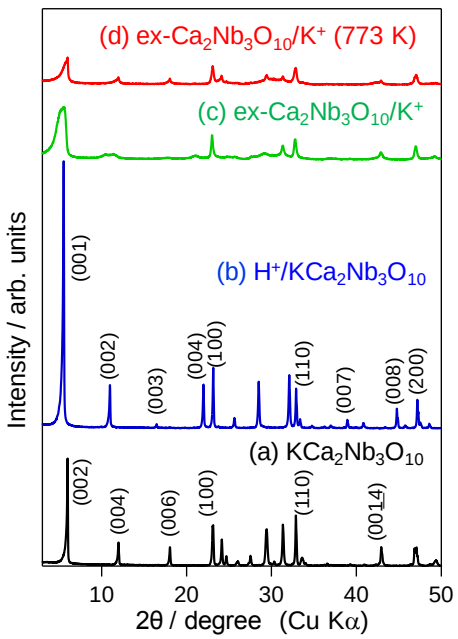

Fig.1 XRD patterns of (a) $KCa_2Nb_3O_{10}$, (b) $H^+/KCa_2Nb_3O_{10}$, (c) ex-$Ca_2Nb_3O_{10}/K^+$ and (d) ex-$Ca_2Nb_3O_{10}/K^+$ (773 K).

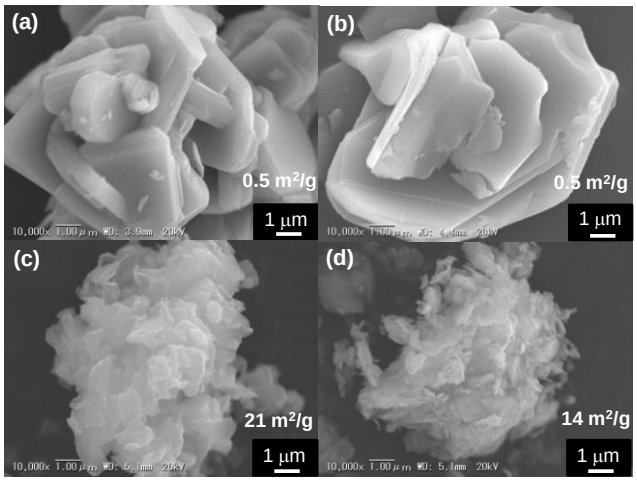

Fig. 2 SEM images of (a) $KCa_2Nb_3O_{10}$, (b) $H^+/KCa_2Nb_3O_{10}$, (c) ex-$Ca_2Nb_3O_{10}/K^+$, (d) ex-$Ca_2Nb_3O_{10}/K^+$ (773 K) particles.

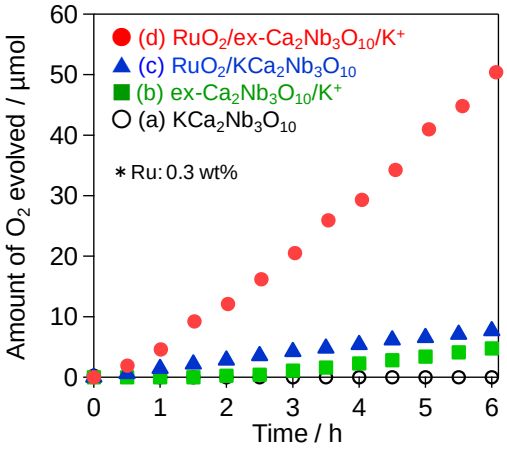

Fig. 3 Time courses of O_2 evolution over 100 mg of (a) $KCa_2Nb_3O_{10}$, (b) ex-$Ca_2Nb_3O_{10}/K^+$, (c) $RuO_2/KCa_2Nb_3O_{10}$, (d) RuO_2/ex-$Ca_2Nb_3O_{10}/K^+$ in 5 mM $NaIO_3$ aqueous solution under UV light irradiation (λ > 300 nm, Xe lamp).

bounded layered structures (see Fig. S1 for TEM image of exfoliated nano sheet and re-stacked one). As shown in Fig. 2-c, the ex-$Ca_2Nb_3O_{10}/K^+$ sample indeed consisted of randomly stacked thin plates with much smaller size (several hundred nanometers) compared to the original one. Through the exfoliation-restack process, the specific surface area of sample significantly increased (from ca. 0.5 to 21 m^2/g, see the values shown in SEM images). This significant increase indicated the increased fraction of outermost layer *via* the exfoliation-restack process and also suggested the formation of pore or voids between the niobate sheets, to which N_2 probe molecules can penetrate. Both the broadening and the shift of (00*n*) peaks toward lower angles in ex-$Ca_2Nb_3O_{10}/K^+$ strongly suggested that the interlayer spaces contained larger amounts of water molecules than in the $H^+/KCa_2Nb_3O_{10}$ sample, possibly along with a small amount of bulky TBA^+ cations that were incorporated during the restack process. While the (00*n*) peaks of the ex-$Ca_2Nb_3O_{10}/K^+$ sample became shaper after calcinations of at 773 K in air certainly due to the elimination of water and TBA^+ molecules from the interlayer spaces, they were readily broadened again by exposing to moisture condition as shown in Fig. S2, indicating facile hydration nature of the interlayer spaces of samples obtained *via* the exfoliation-restack process. On the other hand, the diffraction peaks corresponding to (*lm*0), such as (100) or (110), are clearly remained even after the exfoliation-restack process, while the intensity decreased to be about half of the originals. The clear presence of peaks corresponding to (*lm*0) indicated that the planer structures of niobate sheets themselves were retained to some extent, while the size of sheets was reduced during the exfoliation process, as clearly observed in the SEM and TEM images of ex-$Ca_2Nb_3O_{10}/K^+$ (Fig. 2-c and Fig.S1-b).

3-2. Photocatalytic water oxidation on $KCa_2Nb_3O_{10}$-based samples using IO_3^- as electron acceptor

Fig. 3 shows the time courses of O_2 evolution from water on $KCa_2Nb_3O_{10}$-based samples using iodate (IO_3^-) as an electron acceptor under UV light irradiation. Although O_2 evolution on the original $KCa_2Nb_3O_{10}$ sample was negligible, the ex-$Ca_2Nb_3O_{10}/K^+$ was found to generate appreciable amount of O_2 with steady rate. The proton-exchanged form ($H^+/KCa_2Nb_3O_{10}$) also showed negligibly low activity for O_2 evolution, while the ex-$Ca_2Nb_3O_{10}/K^+$ sample treated with acid (ex-$Ca_2Nb_3O_{10}/K^+/H^+$) generated appreciable amount of O_2 (see Fig. S3). Since the IO_3^- anion cannot penetrate into the interlayer spaces of $KCa_2Nb_3O_{10}$ (or $H^+/KCa_2Nb_3O_{10}$) owing to both the larger size of IO_3^- anions and the electrostatic repulsion between IO_3^- and the negatively charged niobate layers, i.e., $(Ca_2Nb_3O_{10})^-$; the reduction of IO_3^- by the photoexited electrons must occur at the outermost layer or at the edge of niobate layers of $KCa_2Nb_3O_{10}$ (or $H^+/KCa_2Nb_3O_{10}$). Therefore the rate of IO_3^- reduction on $KCa_2Nb_3O_{10}$ is undoubtedly limited by the small amount of the active sites, resulting in the negligibly low rate of water oxidation, due to the fast recombination between electrons and holes. It is reasonable to consider that the O_2 evolution on ex-$Ca_2Nb_3O_{10}/K^+$ sample was enhanced by the increased number of active sites for IO_3^- reduction, based on the fact that the exfoliation-restacking process obviously increased the number of outermost layer and edges of niobate sheets as proven by the increased specific surface area and the SEM images of ex-$Ca_2Nb_3O_{10}/K^+$. The loading of RuO_2 cocatalyst on the surface of $KCa_2Nb_3O_{10}$ particles also increased the rate of O_2 generation (see Fig. 3-c), probably due to the enhanced IO_3^- reduction *via* 6-electron process (eq. 1) on the RuO_2 cocatalysts as reported in the O_2 generation on WO_3 photocatalysts with IO_3^- electron acceptor.[41]

$$IO_3^- + 3H_2O + 6e^- \rightarrow I^- + 6OH^- \quad (1)$$

Combination of the exfoliation-restack process and the loading of RuO_2 cocatalyst drastically increased the rate of O_2 evolution

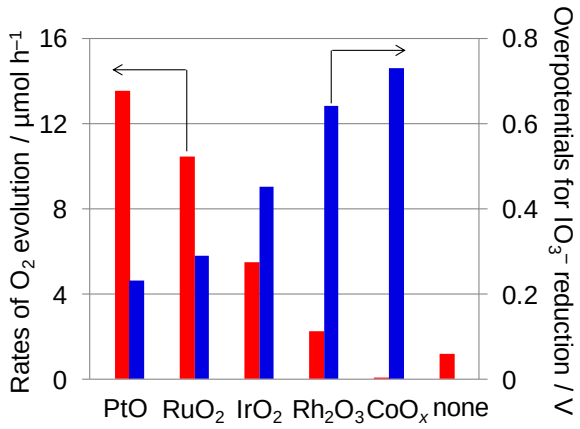

Fig. 4 Rates of O_2 evolution over ex-$Ca_2Nb_3O_{10}/K^+$ loaded with 0.3 wt% of various metal oxides (PtO, RuO_2, IrO_2, Rh_2O_3, CoO_x) in 5 mM $NaIO_3$ aqueous solution under UV light irradiation (λ > 300 nm, Xe lamp) and overpotentials for IO_3^- reduction on each catalyst.

(see Fig. 3-d). This significant increase in O_2 evolution rate is undoubtedly due to the much further enhanced IO_3^- reduction at large number of active sites, i.e., the RuO_2 cocatalysts loaded on the surface of niobate sheets, to which IO_3^- anion can readily access.

The O_2 evolution on ex-$Ca_2Nb_3O_{10}/K^+$ samples loaded with other metal oxides (MO_y) was also evaluated in the presence of IO_3^- as an electron accepter. The rates of O_2 evolution in the steady state were summarized in Fig. 4 as red bars (see Fig. S4 for the time courses). Although the loading of CoO_x was detrimental to the O_2 evolution, all the other cocatalysts were found to increase the rate of O_2 evolution on the ex-$Ca_2Nb_3O_{10}/K^+$ samples. The O_2 evolution rate increased in the following order; Rh_2O_3 < IrO_2 < RuO_2 < PtO. The role of cocatalysts loaded on semiconductor photocatalyst is generally understood as facilitator of the surface redox reactions in reductive and/or oxidative processes, i.e., reduction of IO_3^- and/or oxidation of water in the present reaction system. In order to clarify which process was more facilitated by the effective cocatalysts, electrochemical measurements were carried out on the MO_y particle, which were loaded on conductive glass electrode (FTO) *via* basically same procedure to that on the ex-$Ca_2Nb_3O_{10}/K^+$ samples. Fig. 5 shows CV profiles of FTO substrates loaded with various MO_y, along with unmodified one, in the presence of IO_3^- (10 mM). Although the loading of CoO_x on FTO had almost no effect, the loading of other MO_y, specifically PtO and RuO_2, drastically increased the cathodic current, suggesting the catalytic activity of these MO_y for IO_3^- reduction. Since it was quite difficult to standardize the effective surface area of MO_y particles loaded on FTO, which undoubtedly affects the current value, the catalytic activity of each material was compared by estimating the overpotential for IO_3^- reduction. To estimate the overpotentials for IO_3^- reduction on each catalyst, CV profiles were examined in the absence and in the presence of different concentrations of IO_3^-. As shown in Fig. 6 for example, the onset of cathodic current for IO_3^- reduction on RuO_2/FTO was observed at around 0.79 V vs. RHE. The apparent overpotential on RuO_2/FTO was thus estimated to be ca. 0.30 V from the difference between the onset potential (indicated by the solid line) and the standard redox potential ($E(IO_3^-/I^-)$ = 1.085 V at pH 6.8, as indicated by the dotted line in Fig. 6). As summarized in Fig. 4 as blue bars, the overpotential decreased in the following order; CoO_x > Rh_2O_3 > IrO_2 > RuO_2 > PtO. Cleary, the rate of O_2 evolution on ex-$Ca_2Nb_3O_{10}/K^+$ samples loaded with these MO_y cocatalysts increased with the decreased overpotentials for IO_3^- reduction on the MO_y. On the other hand, clear relationship could not be observed between the O_2 evolution rate and the overpotentials for water oxidation on the MO_y (see Fig. S5). These results indicate that the determining step in this reaction system is the reduction of IO_3^- and thus the activation of this step is key to

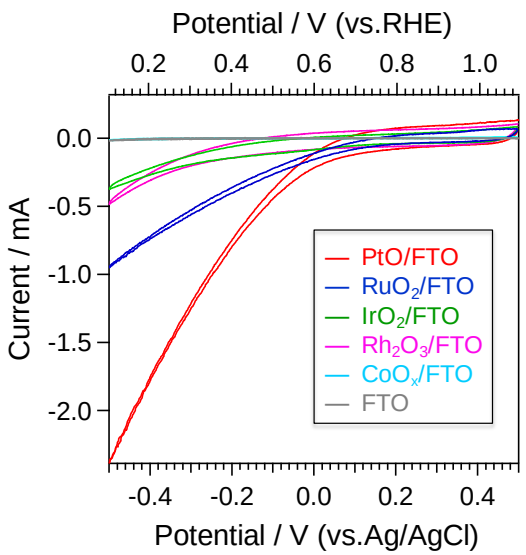

Fig. 5 CV profiles of FTO substrates loaded with various metal oxides in the presence of IO_3^- (10 mM, pH 6.8).

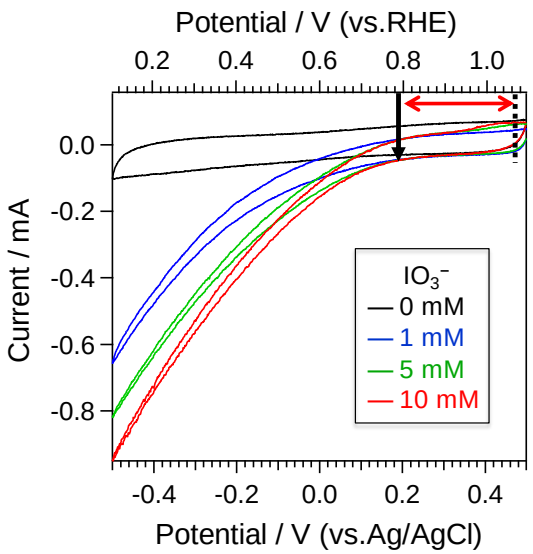

Fig. 6 CV profiles of RuO_2/FTO in the presence of different concentration of IO_3^- (0, 1, 5, 10 mM, pH6.8).

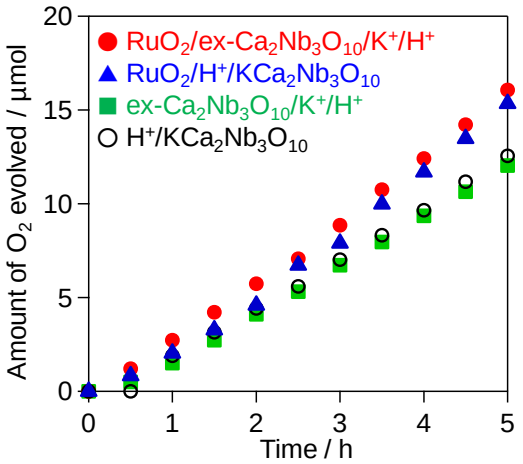

Fig. 7 Time courses of O_2 evolution over 50 mg of $H^+/KCa_2Nb_3O_{10}$, ex-$Ca_2Nb_3O_{10}/K^+/H^+$, $RuO_2/H^+/KCa_2Nb_3O_{10}$, RuO_2/ex-$Ca_2Nb_3O_{10}/K^+/H^+$ in $Fe(NO_3)_3$ aqueous solution (5 mM, pH2.3) under UV light irradiation (λ > 300 nm, Xe lamp).

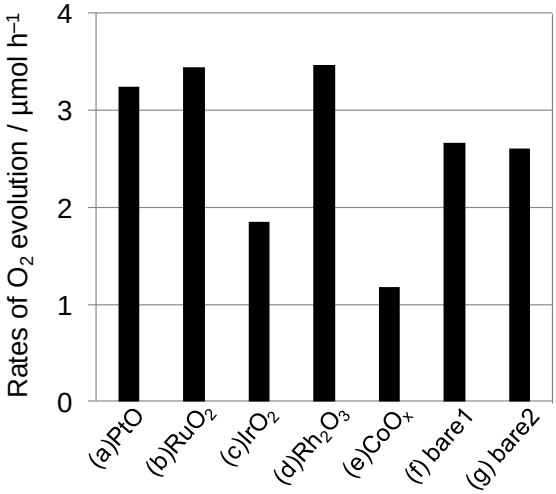

Fig. 8 Rates of O_2 evolution over ex-$Ca_2Nb_3O_{10}/K^+/H^+$ loaded with 0.5 wt% of various metal oxides (PtO, RuO_2, IrO_2, Rh_2O_3, CoO_x) (a~e) and unloaded samples, (f) ex-$Ca_2Nb_3O_{10}/K^+/H^+$ and (g) $H^+/KCa_2Nb_3O_{10}$ in 5 mM $Fe(NO_3)_3$ aqueous solution under UV light irradiation (λ > 300 nm, Xe lamp).

achieve efficient O_2 evolution on the ex-$Ca_2Nb_3O_{10}/K^+$ photocatalysts similar to the case of WO_3 photocatalysts,[41] while one cannot exclude the possibility that these MO_y cocatalysts partially affected the oxidation of water to O_2.

3-3. Photocatalytic water oxidation on $KCa_2Nb_3O_{10}$-based samples using Fe^{3+} as electron acceptor

Photocatalytic O_2 evolution on these $KCa_2Nb_3O_{10}$ derivatives was also examined using Fe^{3+} as an electron acceptor, instead of IO_3^-. In this case, the reaction must be carried out in acidic condition with pH below ca. 3, because Fe^{3+} cations easily precipitate as $Fe(OH)_3$ with higher pH. Thus, the $KCa_2Nb_3O_{10}$–derivatives were treated by HNO_3aq. before the use to replace K^+ by H^+, as well as the addition of an appropriate amount of HNO_3aq. into $Fe(NO_3)_3$aq. for pH adjustment (from 1.5 to 2.5) before each reaction as needed. Fig. 7 shows the time courses of O_2 evolution over $H^+/KCa_2Nb_3O_{10}$, ex-$Ca_2Nb_3O_{10}/K^+/H^+$, and RuO_2-loaded samples under UV light irradiation. Contrary to the case of reactions with IO_3^- acceptor, the layered $H^+/KCa_2Nb_3O_{10}$ sample, which was prepared from $KCa_2Nb_3O_{10}$ *via* simple proton exchange, showed appreciable O_2 evolution in the presence of Fe^{3+}. The rate of O_2 evolution on ex-$Ca_2Nb_3O_{10}/K^+/H^+$ sample, which was prepared *via* exfoliation-restack process and following proton-exchange, was almost same as that on the original $H^+/KCa_2Nb_3O_{10}$, in spite of the marked increase in the specific surface areas (0.5 and 20 m^2/g). These findings strongly suggested that the interlayer spaces of the original $H^+/KCa_2Nb_3O_{10}$ can work as effective reaction sites for reduction of Fe^{3+} because there is possibility that cationic species such as Fe^{3+} are able to intercalate into the interlayer spaces *via* ion-exchange with H^+. The loading of RuO_2 cocatalyst on both the $H^+/KCa_2Nb_3O_{10}$ and ex-$Ca_2Nb_3O_{10}/K^+/H^+$ samples obviously increased the rate of O_2 generation compared to the original ones; however the enhancement was not so significant compared to that in the case of IO_3^- acceptor (see Fig. 3). The effect of MO_y cocatalyst on the O_2 evolution was also examined on the ex-$Ca_2Nb_3O_{10}/K^+/H^+$ samples in the presence of Fe^{3+} electron acceptor. As summarized in Fig. 8, the loading of PtO and Rh_2O_3 appreciably enhanced the rate of O_2 evolution, while the enhancement was not so remarkable. The electrochemical measurement on these MO_y loaded on FTO was also carried out to evaluate the catalytic activity for reduction of Fe^{3+}. Although the cathodic current obviously increased on all the metal oxides except for CoO_x (see Fig. S6), the onset potentials for Fe^{3+} reduction were observed at similar potentials at around 0.5 V vs. Ag/AgCl; suggesting that the overpotentials for Fe^{3+} reduction on these materials are quite small. Because the reduction of Fe^{3+} to Fe^{2+} is one-electron process, this reaction is expected to proceed with relatively-high efficiency even without effective cocatalysts, i.e., even on the bare surface and/or in the interlayers of $H^+/KCa_2Nb_3O_{10}$ based materials. Indeed, the unmodified samples such as ex-$Ca_2Nb_3O_{10}/K^+/H^+$ showed relatively high rate of O_2 evolution with steady rate (see Fig. 7). Thus, the loading of cocatalysts had a limited effect for enhancing O_2 evolution on the ex-$Ca_2Nb_3O_{10}/K^+/H^+$ photocatalysts with Fe^{3+} acceptor.

3-4. Z-scheme type water splitting using $KCa_2Nb_3O_{10}$ derivatives as O_2-evolving photocatalysts coupled with a H_2-evolving photocatalyst in the presence of IO_3^-/I^- or Fe^{3+}/Fe^{2+} redox

Overall water splitting (i.e., simultaneous evolution of H_2 and O_2) was attempted by combining the $KCa_2Nb_3O_{10}$ derivatives with an appropriate H_2-evolving photocatalyst in the presence of IO_3^-/I^- or Fe^{3+}/Fe^{2+} redox. In the present study, strontium titanate ($SrTiO_3$) doped with Rh species (denoted as $SrTiO_3$:Rh)

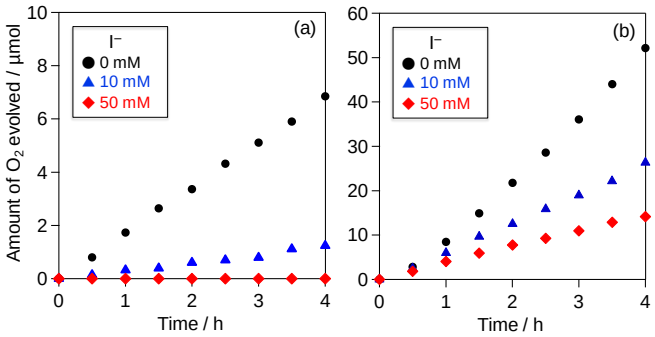

Fig. 9 Time courses of O_2 evolution over (a) PtO(0.5 wt%)/$KCa_2Nb_3O_{10}$, (b) PtO(0.5 wt%)/ex-$Ca_2Nb_3O_{10}/K^+$, in the solution containing different concentration of I^- (0 – 50 mM) and a fixed concentration of IO_3^- (5 mM) at pH 9.6.

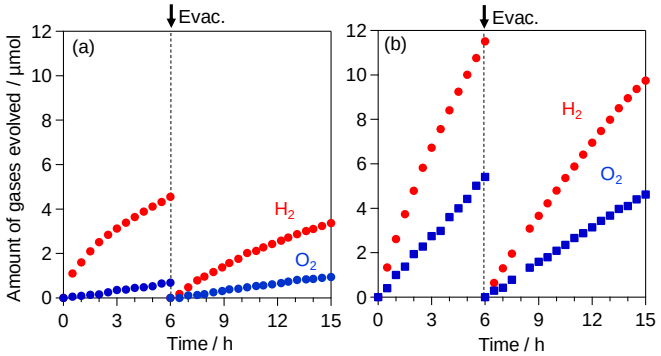

Fig. 10 Time courses of H_2 and O_2 evolution using a mixture of Pt(0.5 wt%)/$SrTiO_3$:Rh and PtO(0.5 wt%)/$KCa_2Nb_3O_{10}$ (a) or PtO(0.5 wt%)/ex-$Ca_2Nb_3O_{10}/K^+$ (b) KI aqueous solution (5 mM, pH 12.0) under UV light irradiation (λ > 300 nm, Xe lamp).

was used as the H_2-evolution photocatalyst, which had been first reported by Kudo *et al*. to show reasonable activity for H_2-evolution in the presence of Fe^{2+} electron donor under visible light.[9] We also confirmed that the $SrTiO_3$:Rh loaded with Pt cocatalysts can generate H_2 from aqueous solution containing I^- as an electron donor both under UV and visible light irradiation (see Fig. S7); no O_2 generation was observed even under UV light irradiation. Before constructing Z-scheme systems for simultaneous evolution of H_2 and O_2, the selectivity for water oxidation on the $KCa_2Nb_3O_{10}$ derivatives was evaluated in the coexistence of an electron acceptor (i.e., IO_3^- or Fe^{3+}) and an electron donor (i.e., I^- or Fe^{2+}). Although high concentration of electron donor is generally required for achieving efficient H_2 generation on H_2-evolving photocatalyst, it adversely decrease the rate of O_2 evolution on O_2-evolving photocatalyst primary due to the occurrence of competitive backward reaction, i.e., the oxidation of the electron donor in place of oxidation of water.[42-44] Thus, high selectivity for water oxidation, i.e., the capability of O_2 evolution even in the presence of considerable concentration of electron donor (I^- or Fe^{2+}), is required for the O_2-evolving photocatalysts that are employed in Z-scheme water splitting systems.

Fig. 9 shows the rates of O_2 evolution over PtO/ex-$Ca_2Nb_3O_{10}/K^+$ and PtO/$KCa_2Nb_3O_{10}$ samples from the solution containing different concentration of I^- (0 – 50 mM) and a fixed concentration of IO_3^- (5 mM). On the both samples, the O_2 evolution rates significantly decrease with increasing concentration of I^- in the solution, undoubtedly due to the occurrence of backward reaction (the oxidation of I^-) instead of oxidation of water to O_2. The O_2 evolution rate on PtO/ex-$Ca_2Nb_3O_{10}/K^+$ sample was reduced to about one-half by the addition of 10 mM of I^- to the solution, while that on PtO/$KCa_2Nb_3O_{10}$ was reduced to almost one-fifth of that in the absence of I^-. These findings indicated that PtO/ex-$Ca_2Nb_3O_{10}/K^+$ sample possess relatively high selectivity for water oxidation, and therefore can be used as O_2-evolving photocatalyst with an appropriate concentration of I^- electron donor lower than 10 mM, while the original PtO/$KCa_2Nb_3O_{10}$ sample should be used with much lower concentration of I^- below 1 mM.

Then, simultaneous evolution of H_2 and O_2 was attempted by combining these $KCa_2Nb_3O_{10}$ derivatives with the $SrTiO_3$:Rh loaded with Pt cocatalysts in an aqueous KI solution (5 mM). The concentration of KI (5 mM) was chosen based on the fact that the rate of H_2 evolution on Pt/$SrTiO_3$:Rh photocatalyst increased with the increasing concentration up to

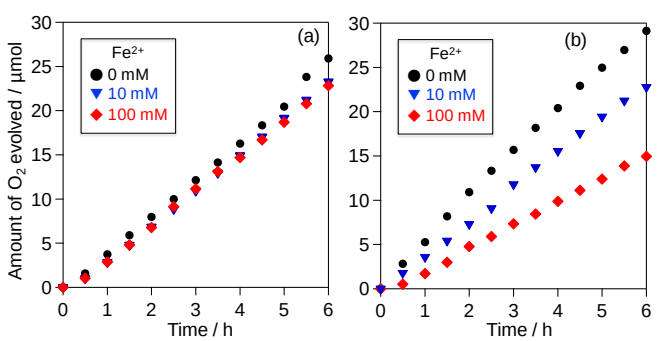

Fig. 11 Time courses of O_2 evolution over (a) $H^+/KCa_2Nb_3O_{10}$, (b) ex-$Ca_2Nb_3O_{10}/K^+/H^+$ in the solution containing different concentration of Fe^{2+} (0 – 100 mM) and a fixed concentration of Fe^{3+} (5 mM) at pH 1.5.

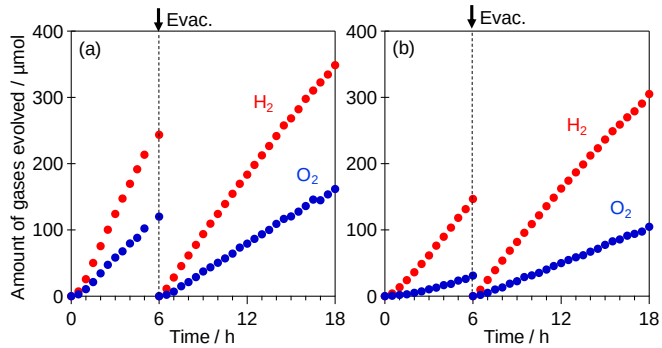

Fig. 12 Time courses of H_2 and O_2 evolution using a mixture of Ru(0.7 wt%)/$SrTiO_3$:Rh and $H^+/KCa_2Nb_3O_{10}$ (a) or ex-$Ca_2Nb_3O_{10}/K^+/H^+$ (b) in $Fe(ClO_4)_2$ aqueous solution (5 mM, pH 2.5) under UV light irradiation (λ > 300 nm, Xe lamp).

5 mM and almost saturated at higher concentrations. As shown in Fig. 10a, the combination of PtO/ex-$Ca_2Nb_3O_{10}/K^+$ and Pt/$SrTiO_3$:Rh resulted in simultaneous and stable evolution of H_2 and O_2 in the stoichiometric ratio (2:1). Such simultaneous evolution was not observed when the each photocatalyst was singly irradiated under same condition. No steady gas evolution proceeded in the absence of I^-. These findings indicated that the water splitting into H_2 and O_2 proceeded through two-step photoexcitation between these two different photocatalysts. Although the use of PtO/$KCa_2Nb_3O_{10}$ with Pt/$SrTiO_3$:Rh resulted in simultaneous evolution of H_2 and O_2 as seen in Fig. 10b, the amount of O_2 was obviously lower than the stoichiometric value expected by the amount of H_2 generated. This deviation is certainly due to both the low activity and selectivity for water oxidation of PtO/$KCa_2Nb_3O_{10}$ sample, as indicated by the result shown in Fig. 9.

The construction of Z-scheme water splitting system with Fe^{3+}/Fe^{2+} redox was also attempted using the $KCa_2Nb_3O_{10}$ derivatives as O_2-evolving photocatalysts. To suppress the precipitation of Fe^{3+} into $Fe(OH)_3$ under higher pH condition than ca. 3, the $KCa_2Nb_3O_{10}$ derivatives were used after exchanging the K^+ cations by H^+ as described in a previous section. Fig. 11 shows the rates of O_2 evolution over $H^+/KCa_2Nb_3O_{10}$ and ex-$Ca_2Nb_3O_{10}/K^+/H^+$ samples from the solution containing different concentration of Fe^{2+} (0 – 100 mM) and a fixed concentration of Fe^{3+} (5 mM). Because the aqueous solutions containing high concentration of $Fe(ClO_4)_2$ themselves exhibit pH values below 2, all the pH values of the reaction solution (containing catalyst particles) were adjusted to 1.5 by adding appropriate amounts of $HClO_4$aq. to minimize the influence of pH difference on the O_2 evolution. Interestingly, the rate of O_2 evolution on $H^+/KCa_2Nb_3O_{10}$ was rarely affected by the increasing concentration of Fe^{2+} electron donor in the solution, indicating the high selectivity for water oxidation on this sample. On the other hand, the rate of O_2 evolution on ex-$Ca_2Nb_3O_{10}/K^+/H^+$ sample appreciably decreased with increasing concentration of Fe^{2+}, strongly suggesting the occurrence of backward reaction (oxidation of Fe^{2+}) on this catalyst. One of the most likely reasons for the selective oxidation of water on the original $H^+/KCa_2Nb_3O_{10}$ sample even in the presence of considerable amount of Fe^{2+} will be the preferential intercalation of Fe^{3+} cations instead of Fe^{2+} into the active interlayer spaces. Considering the size of Fe^{3+} and Fe^{2+} cations, the larger size of Fe^{2+} certainly makes it difficult for the Fe^{2+} cations to stay in the narrow interlayer spaces, resulting in the elimination of them from the interlayers, whereas smaller Fe^{3+} can be there. In that case, the photoexcited electrons generated on 2-dimentional niobate sheet can efficiently reduce Fe^{3+} cations that are intercalated into the interlayer space, whereas the photogenerated holes can selectively oxidize water in the interlayer space where the Fe^{2+} cations are excluded. Although the clear clues for preferential intercalation of Fe^{3+} rather than Fe^{2+} could not be obtained in the present materials mainly due to the competitive exchange with H^+ cations in the acidic condition, such preferential intercalation probably can be an effective way to achieve highly efficient O_2 evolution in the two-step water splitting systems with Fe^{3+}/Fe^{2+} redox couple.

Water splitting into H_2 and O_2 was attempted by combining these O_2-evolving photocatalyst with $SrTiO_3$:Rh loaded with Ru cocatalyst[11] in an aqueous $Fe(ClO_4)_2$ solution (5 mM, pH 2.5) under UV and visible light irradiation (λ > 300 nm). As shown in Fig. 12a, the combination of $H^+/KCa_2Nb_3O_{10}$ and Ru/$SrTiO_3$:Rh generated H_2 and O_2 with the stoichiometric rate quite stably for long time. On the other hand, the use of ex-$Ca_2Nb_3O_{10}/K^+/H^+$ sample resulted in the smaller amount of O_2 than stoichiometric amount as seen in Fig. 12b, undoubtedly due to the occurrence of backward reaction (oxidation of Fe^{2+}) on ex-$Ca_2Nb_3O_{10}/K^+/H^+$ as demonstrated in the half reactions (Fig. 11). These findings indicate the potential availability of cation-exchangeable layered materials as efficient O_2-evolving photocatalysts for achieving efficient water splitting in the Fe^{3+}/Fe^{2+} redox mediator.

4. Conclusions

In the present study, we attempted to apply a cation-exchangeable layered semiconductor $KCa_2Nb_3O_{10}$ and its derivatives as O_2-evolving photocatalyst in Z-scheme type water splitting systems with redox mediators, IO_3^-/I^- and Fe^{3+}/Fe^{2+}. The optimum form of the photocatalyst materials was found to strongly depend on the redox couples combined. When IO_3^- was used as an electron acceptor for O_2 evolution, combination of the exfoliation-restacking process and the loading of appropriate cocatalysts such as PtO were quite effective to increase the rate of O_2 evolution. The former one can effectively increase the numbers of the opened active sites where the large and anionic IO_3^- can access, and the later one significantly catalyzes the reduction of IO_3^-, which proceed *via* 6-electrons process. On the other hand, the original layered structure of $H^+/KCa_2Nb_3O_{10}$ sample, which was obtained *via* simple proton exchange of $KCa_2Nb_3O_{10}$, was effective for achieving efficient and selective water oxidation to O_2 in the presence of Fe^{3+} electron acceptor; the exfoliation-restacking process adversely lowered the selectivity. These findings strongly suggested that the caiton-exchangeable interlayer spaces could work as effective reaction sites for reduction of Fe^{3+}. Simultaneous and stoichiometric evolutions of H_2 and O_2 with were indeed demonstrated under UV light irradiation by employing the optimum $KCa_2Nb_3O_{10}$-based material as an O_2-evolving photocatalyst combined with a H_2-evolving photocatalyst with an appropriate redox couple. The present results indicated potential availability of cation-exchangeable metal oxides as efficient photocatalysts materials affording high selectivity for water reduction and/or oxidation in Z-scheme type water splitting systems with redox couple.

Acknowledgements

This work was financially supported by the JST-CREST and the JSPS-NEXT program. The authors are also indebted to the technical division of Catalysis Research Center, Hokkaido

University for their help in building the experimental equipment.

Notes and references

1 R. Abe, K. Sayama, K. Domen and H. Arakawa, *Chem. Phys. Lett.*, 2001, **344**, 339-344.
2 R. Abe, T. Takata, H. Sugihara and K. Domen, *Chem. Commun.*, 2005, 3829-3831.
3 M. Higashi, R. Abe, A. Ishikawa, T. Takata, B. Ohtani and K. Domen, *Chem. Lett.*, 2008, **37**, 138-139.
4 M. Higashi, R. Abe, K. Teramura, T. Takata, B. Ohtani and K. Domen, *Chem. Phys. Lett.*, 2008, **452**, 120-123.
5 M. Higashi, R. Abe, T. Takata and K. Domen, *Chem. Mater.*, 2009, **21**, 1543-1549.
6 K. Maeda, M. Higashi, D. L. Lu, R. Abe and K. Domen, *J. Am. Chem. Soc.*, 2010, **132**, 5858-5868.
7 R. Abe, K. Shinmei, K. Hara and B. Ohtani, *Chem. Commun.*, 2009, 3577-3579.
8 R. Abe, K. Shinmei, N. Koumura, K. Hara and B. Ohtani, *J. Am. Chem. Soc.*, 2013, **135**, 16872-16884.
9 H. Kato, M. Hori, R. Konta, Y. Shimodaira and A. Kudo, *Chem. Lett.*, 2004, **33**, 1348-1349.
10 H. Kato, Y. Sasaki, A. Iwase and A. Kudo, *Bull. Chem. Soc. Jpn.*, 2007, **80**, 2457-2464.
11 Y. Sasaki, A. Iwase, H. Kato and A. Kudo, *J. Catal.*, 2008, **259**, 133-137.
12 Y. Sasaki, H. Kato and A. Kudo, *J. Am. Chem. Soc.*, 2013, **135**, 5441-5449.
13 Y. Sasaki, H. Nemoto, K. Saito and A. Kudo, *J. Phys. Chem. C*, 2009, **113**, 17536-17542.
14 M. Shibata, A. Kudo, A. Tanaka, K. Domen, K. Maruya and T. Onishi, *Chem Lett*, 1987, 1017-1018.
15 J. Yoshimura, Y. Ebina, J. Kondo, K. Domen and A. Tanaka, *J. Phys. Chem.*, 1993, **97**, 1970-1973.
16 A. Kudo and T. Kondo, *J. Mater. Chem.*, 1997, **7**, 777-780.
17 M. R. Allen, A. Thibert, E. M. Sabio, N. D. Browning, D. S. Larsen and F. E. Osterloh, *Chem. Mater.*, 2010, **22**, 1220-1228.
18 K. Domen, Y. Ebina, T. Sekine, A. Tanaka, J. Kondo and C. Hirose, *Catal. Today*, 1993, **16**, 479-486.
19 M. Machida, X. W. Ma, H. Taniguchi, J. Yabunaka and T. Kijima, *J. Mol .Catal. a-Chem.*, 2000, **155**, 131-142.
20 K. Domen, Y. Ebina, S. Ikeda, A. Tanaka, J. N. Konda and K. Maruya, *Catal Today*, 1996, **28**, 167-174.
21 S. Ida, Y. Okamoto, S. Koga, H. Hagiwara and T. Ishihara, *Rsc Adv*, 2013, **3**, 11521-11524.
22 S. Ida, Y. Okamoto, M. Matsuka, H. Hagiwara and T. Ishihara, *J Am Chem Soc*, 2012, **134**, 15773-15782.
23 K. Domen, A. Kudo, A. Shinozaki, A. Tanaka, K. Maruya and T. Onishi, *J. Chem. Soc. Chem. Comm.*, 1986, 356-357.
24 A. Kudo, K. Sayama, A. Tanaka, K. Asakura, K. Domen, K. Maruya and T. Onishi, *J. Catal.*, 1989, **120**, 337-352.
25 A. Kudo, A. Tanaka, K. Domen, K. Maruya, K. Aika and T. Onishi, *J. Catal.*, 1988, **111**, 67-76.
26 T. Takata, Y. Furumi, K. Shinohara, A. Tanaka, M. Hara, J. N. Kondo and K. Domen, *Chem. Mater.*, 1997, **9**, 1063-1064.
27 T. Takata, K. Shinohara, A. Tanaka, M. Hara, J. N. Kondo and K. Domen, *J. Photochem. Photobiol. A*, 1997, **106**, 45-49.
28 K. Sayama, H. Arakawa and K. Domen, *Catal. Today*, 1996, **28**, 175-182.
29 M. Machida, J. Yabunaka and T. Kijima, *Chem. Commun.*, 1999, 1939-1940.
30 M. Machida, J. Yabunaka and T. Kijima, *Chem. Mater.*, 2000, **12**, 812-817.
31 K. Shimizu, S. Itoh, T. Hatamachi, T. Kodama, M. Sato and K. Toda, *Chem. Mater.*, 2005, **17**, 5161-5166.
32 K. Shimizu, Y. Tsuji, T. Hatamachi, K. Toda, T. Kodama, M. Sato and Y. Kitayama, *Phys. Chem. Chem. Phys.*, 2004, **6**, 1064-1069.
33 M. Machida, T. Mitsuyama, K. Ikeue, S. Matsushima and M. Arai, *J. Phys. Chem. B*, 2005, **109**, 7801-7806.
34 H. Kato and A. Kudo, *J. Phys. Chem. B*, 2002, **106**, 5029-5034.
35 T. Ishii, H. Kato and A. Kudo, *J. Photoch. Photobio. A*, 2004, **163**, 181-186.
36 R. Konta, T. Ishii, H. Kato and A. Kudo, *J. Phys. Chem. B*, 2004, **108**, 8992-8995.
37 K. Domen, J. Yoshimura, T. Sekine, A. Tanaka and T. Onishi, *Catal. Lett.*, 1990, **4**, 339-343.
38 Y. Ebina, N. Sakai and T. Sasaki, *J. Phys. Chem. B*, 2005, **109**, 17212-17216.
39 M. Dion, M. Ganne and M. Tournoux, *Mater. Res. Bull.*, 1981, **16**, 1429-1435.
40 A. J. Jacobson, J. T. Lewandowski and J. W. Johnson, *J. Less-Common. Met.*, 1986, **116**, 137-146.
41 R. Abe, M. Higashi and K. Domen, *Chemsuschem*, 2011, **4**, 228-237.
42 R. Abe, *J. Photochem. Photobiol. C*, 2010, **11**, 179-209.
43 R. Abe, *Bull. Chem. Soc. Jpn.*, 2011, **84**, 1000-1030.
44 T. Ohno, D. Haga, K. Fujihara, K. Kaizaki and M. Matsumura, *J. Phys. Chem. B*, 1997, **101**, 6415-6419.

Supporting Information

Two-step photocatalytic water splitting into H_2 and O_2 using layered metal oxide $KCa_2Nb_3O_{10}$ and its derivatives as O_2-evolving photocatalysts with IO_3^-/I^- or Fe^{3+}/Fe^{2+} redox mediator

Hajime Suzuki,[a] Osamu Tomita,[a] Masanobu Higashi,[a] Ryu Abe*[a,b]

[a] *Graduate School of Engineering, Kyoto University, Katsura, Nishikyo-ku, Kyoto 615-8510, Japan*

[b] *JST-CREST, Sanbancho 5, Chiyoda-ku, Tokyo 102-0075, Japan*

E-mail: ryu-abe@scl.kyoto-u.ac.jp

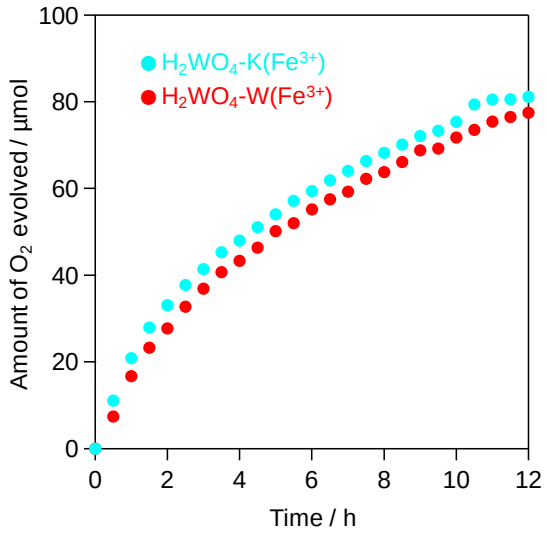

Fig. S1 Time courses of O_2 evolution over H_2WO_4-W and H_2WO_4-K in $Fe(ClO_4)_3$ aqueous solution (5 mM, pH2.3) under visible light irradiation (λ > 400 nm, Xe lamp).

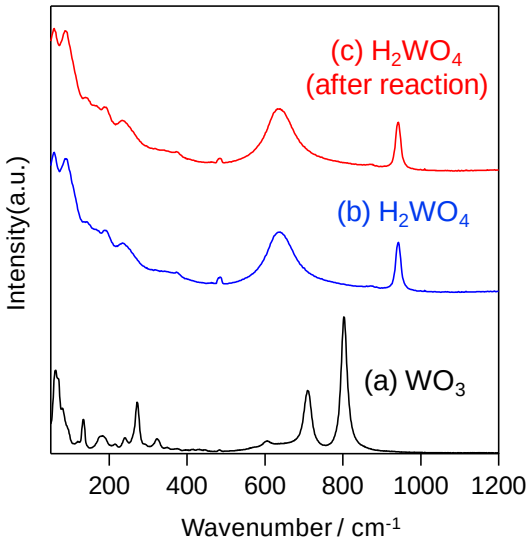

Fig. S2 Raman spectra of (a)WO_3 and (b,c) H_2WO_4 before and after O_2 evolution from $Fe(ClO_4)_3$ aqueous solution.

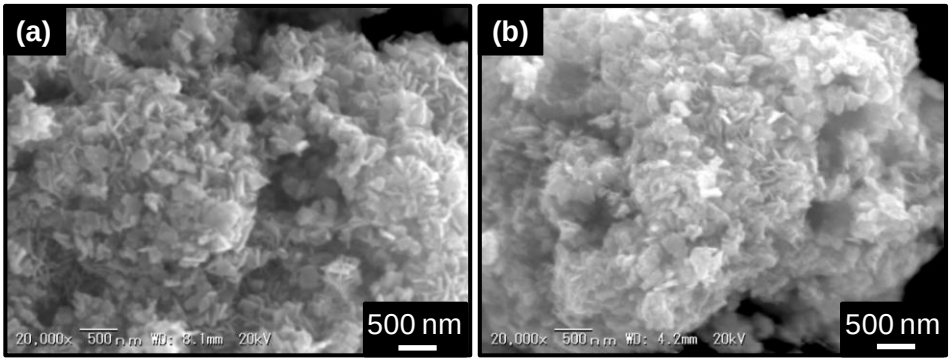

Fig. S3 SEM image of H_2WO_4 (a) before and (b) after O_2 evolution from $Fe(ClO_4)_3$ aqueous solution .